Journal of Materials Chemistry A

Materials for energy and sustainability

www.rsc.org/MaterialsA

Volume 1 | Number 13 | 7 April 2013 | Pages 4121–4392

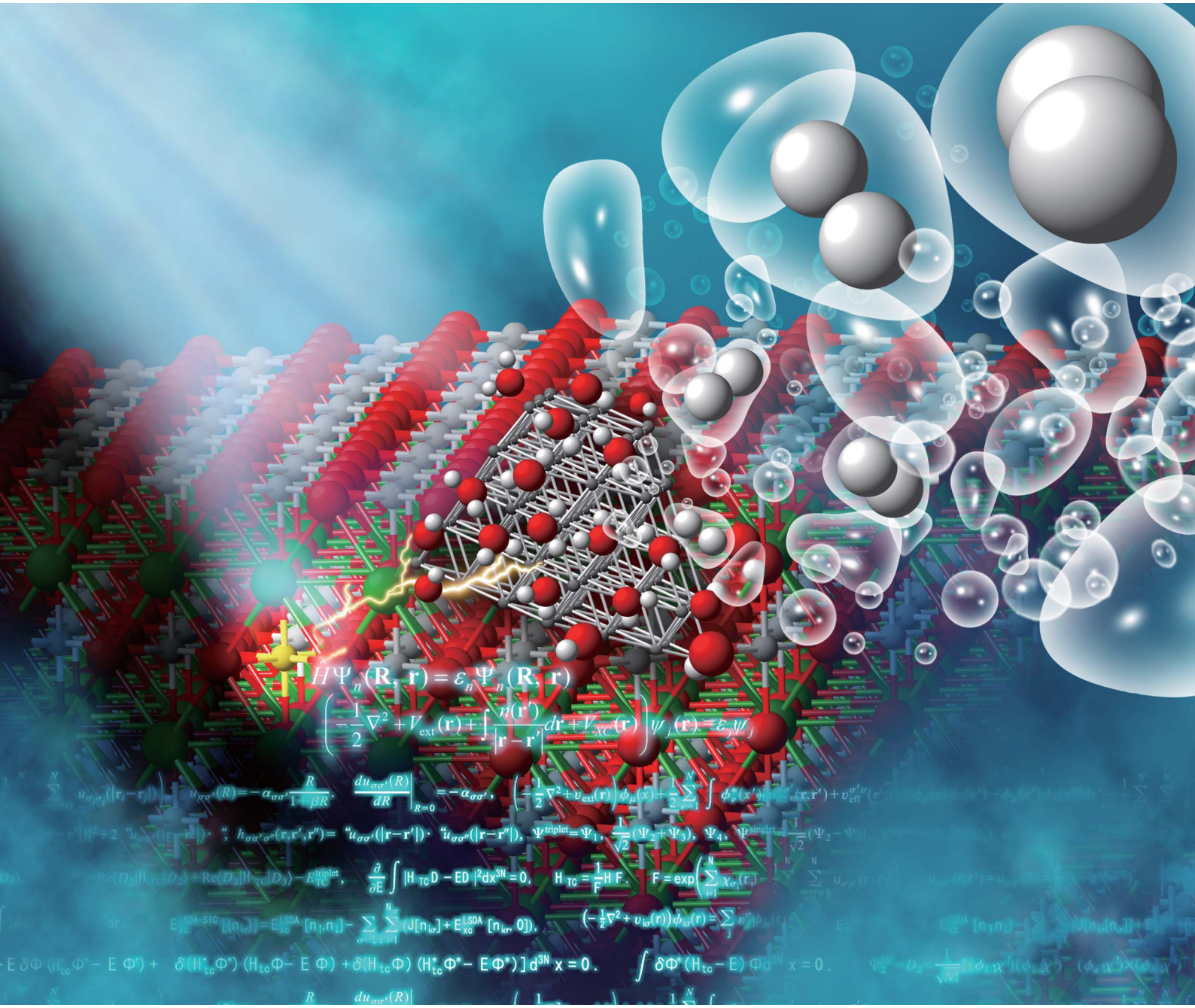

ISSN 2050-7488

RSC Publishing

PAPER

Naoto Umezawa *et al.*

Theoretical design of highly active $SrTiO_3$-based photocatalysts by a codoping scheme towards solar energy utilization for hydrogen production

2050-7488(2013)1:13;1-0

Journal of Materials Chemistry A

RSC Publishing

PAPER

View Article Online
View Journal | View Issue

Cite this: J. Mater. Chem. A, 2013, 1, 4221

Theoretical design of highly active $SrTiO_3$-based photocatalysts by a codoping scheme towards solar energy utilization for hydrogen production†

Pakpoom Reunchan,[ae] Shuxin Ouyang,[a] Naoto Umezawa,*[abd] Hua Xu,[a] Yuanjian Zhang[cf] and Jinhua Ye[acd]

$SrTiO_3$ is a promising photocatalyst for the production of hydrogen from water splitting under solar light. Cr doping is an effective treatment for adjusting its absorption edge to the visible-light range, although the performance of Cr-doped $SrTiO_3$ is strongly affected by the oxidation number of the Cr ions. In this study, we theoretically predict that elevating the Fermi level, *i.e.*, *n*-type carrier doping in $SrTiO_3$, can stabilize the desirable oxidation number of chromium (Cr^{3+}), contributing to a higher activity for H_2 evolution. Our computational results, based on hybrid density-functional calculations, reveal that such an *n*-type condition is realized by substituting group-V metals (Ta, Sb, and Nb), group-III metals (La and Y), and fluorine atoms for the Ti, Sr, and O sites in $SrTiO_3$, respectively. From our systematic study of the capability of each dopant, we conclude that La is the most effective donor for stabilizing Cr^{3+}. This prediction is successfully evidenced by experiments showing that the La and Cr codoped $SrTiO_3$ dramatically increases the amount of H_2 gas evolved from water under visible-light irradiation, which demonstrates that our guiding principle based on Fermi level tuning by the codoping scheme is valid for the design of advanced photocatalysts.

Received 26th September 2012
Accepted 21st December 2012

DOI: 10.1039/c2ta00450j

www.rsc.org/MaterialsA

Introduction

There has recently been much interest in the potential use of photocatalytic materials in the production of clean-energy fuels and the reduction of environmental pollutants.[1] Since the discovery of the Honda–Fujishima effect,[2] TiO_2 has been extensively studied and applied to various commercial products, mainly for decomposing harmful chemicals or antifouling coatings. However, its application to fuel production is still limited due to the insufficient efficiency of overall water splitting for H_2 evolution.[2,3] It is therefore a challenge to find a highly active photocatalyst to meet today's demands for alternative energy resources. The perovskite strontium titanate ($SrTiO_3$ or STO) is a promising photocatalyst because of several advantages, such as high chemical stability and abundance of the constituent elements. The valence-band and conduction-band edges of STO are favorably situated for overall water splitting:[4–7] the valence-band maximum (VBM) is much lower than the oxidation potential of water, and the conduction band minimum (CBM) is ~0.8 eV (at pH = 0) higher than the standard hydrogen electrode potential (SHE).[7] The sufficiently large band offset of the CBM with respect to SHE, which is much larger than that of anatase TiO_2 (0.1–0.2 eV), is a great benefit for the chemical reactions of photoexcited electrons with protons on the surface: $2H^+ + 2e^- \rightarrow H_2$. Nevertheless, the photoabsorption range of STO is restricted to ultra-violet light because of its relatively wide band gap (3.25 eV), and the majority of sunlight, *i.e.* visible light is hardly utilized in photocatalytic reactions on pristine STO. One approach to overcome this problem is to induce a red-shift of the absorption edge while keeping the position of the CBM unchanged, in order to maintain its potential for proton reduction. Chromium (Cr) is of particular interest as an effective dopant for activating visible-light absorption in wide-gap semiconductor oxides.[8–14] In fact, Cr-doped STO can work continuously and stably under visible light for more than 500 hours, and therefore possesses

[a]Environmental Remediation Materials Unit, National Institute for Materials Science (NIMS), 1-1 Namiki, Tsukuba, Ibaraki 305-0044, Japan. E-mail: Umezawa.Naoto@nims.go.jp

[b]PRESTO, Japan Science and Technology Agency (JST), 4-1-8 Honcho, Kawaguchi, Saitama 332-0012, Japan

[c]International Center for Materials Nanoarchitectonics (MANA), National Institute for Materials Sciences, Ibaraki 305-0047, Japan

[d]TU-NIMS Joint Research Center, School of Materials Science and Engineering, Tianjin University, 92 Weijin Road, Nankai District, Tianjin, P. R. China

[e]Department of Physics, Faculty of Science, Kasetsart University, Bangkok 10900, Thailand. E-mail: pakpoom.r@ku.ac.th

[f]School of Chemistry and Chemical Engineering, Southeast University, Nanjing 211189, China

† Electronic supplementary information (ESI) available: details of sample synthesis and experimental details for photocatalytic H_2 evolution, XPS measurements, and optical absorption spectra for the selected codoped $SrTiO_3$. The calculated density of states for the supercell containing Cr defects and the supercell containing donor-type codopant defects. See DOI: 10.1039/c2ta00450j

great potential for future solar hydrogen production.[10,12] Importantly, Cr-doped STO is active only when the Cr ions possess a lower oxidation number (Cr^{3+}), while it is inactive for higher oxidation states of Cr.[11,12] Thus, the stabilization of Cr^{3+} is a key strategy for enhancing the photocatalytic performance of Cr-doped photocatalysts.

Recently, we have theoretically shown that the desirable oxidation state Cr^{3+} predominates in *n*-type STO,[15] namely the condition at which the Fermi level (ε_F) is located near the CBM. The negatively charged substitutional Cr at the titanium site (Cr_{Ti}^{-}), which was identified as the source of Cr^{3+} in Cr-doped STO, gives rise to fully occupied states above the VBM. Fig. 1(a) shows schematically the electronic structures associated with substitutional Cr at a Ti site with two different charge states (Cr_{Ti}^{0} and Cr_{Ti}^{-}). In a low ε_F condition, the neutral charge state Cr_{Ti}^{0}, which corresponds to a high oxidation state of the Cr ion, is stabilized and photo-exited electrons are likely to be trapped in unoccupied gap states, degrading photocatalytic reactions. By contrast, shifting ε_F towards the conduction band eliminates the trapping centers due to the realization of the desirable charge state Cr_{Ti}^{-}. Our computational results revealed that the occupied gap states associated with Cr_{Ti}^{-} play an important role both in the photoresponse under visible light and in the elimination of electron trapping centers.[15]

Previously, some experimental reports showed that the photocatalytic performance of Cr-doped STO is improved by codoping with antimony (Sb),[10] tantalum (Ta),[11] or niobium (Nb),[11] or by pretreatment in a reducing H_2 atmosphere.[11] In all of these treatments, the concentration of Cr^{3+} is expected to increase because of the electron carrier doping upon incorporation of these elements into STO. Although the effect of Cr^{3+} has been clearly addressed in our previous work,[15] knowledge of the role played by codopants is still lacking. Since STO is also a promising semiconductor for oxide electronics,[16,17] carrier doping of this technologically important material is of great interest to a wide range of researchers. In particular, *n*-type doping of this wide band-gap semiconductor is a key target in many different fields of research,[18–21] and the most suitable donor for STO remains to be identified.

Here, we systematically investigate the effects of doping STO with the group-V metals Ta, Sb, Nb, and vanadium (V), the group-III metals lanthanum (La) and yttrium (Y), and the halogen fluorine (F), in order to theoretically identify the most effective donor in STO and the best candidate codopant for stabilizing Cr^{3+} in Cr-doped STO.

The above-mentioned metal dopants can be readily incorporated into the STO lattice thanks to the similarity of their ionic radii to those of the host elements. For instance, the ionic radii of La^{3+} (1.16 Å) and Nb^{5+} (0.64 Å) are very close to those of Sr^{2+} (1.26 Å) and Ti^{4+} (0.61 Å), respectively, that is, the group-V metals preferentially occupy the Ti site rather than the Sr site, while the group-III metals tend to occupy the Sr sites. Our theory, based on hybrid density-functional calculations, predicts that La is the best donor among the candidate elements in terms of electron doping ability and the ability to stabilize Cr^{3+}. The prediction is successfully validated by our experiments, which clearly show that La and Cr codoped STO exhibits the best performance for hydrogen evolution from water splitting under visible-light irradiation among the candidate materials examined in this work.

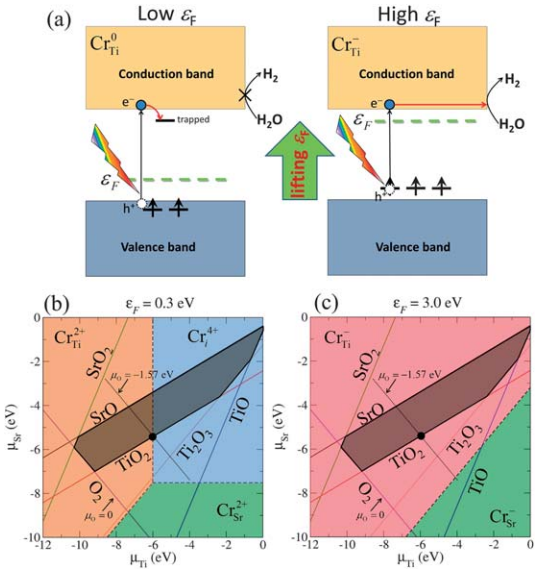

Fig. 1 (a) Schematic illustration of the effect of shifting ε_F towards the conduction band on the stabilization of a low oxidation state of the Cr ion associated with Cr_{Ti}^{-} in Cr-doped STO. The energy levels of the in-gap Cr d states are shown. The arrows indicate the electron occupation corresponding to the associated charge state. (b) and (c) Illustrations of the conditions under which various Cr-related defects are stable, derived from the formation energy, with respect to the chemical potentials of Sr and Ti for (b) $\varepsilon_F = 0.3$ eV (*p*-type STO) and (c) $\varepsilon_F = 3.0$ eV (*n*-type STO). For the growth of STO under thermal equilibrium, μ_{Sr}, μ_{Ti}, and μ_O must lie in the dark-shaded region.

Methods of calculation

Our calculations were based on density-functional theory with the hybrid-functional of Heyd, Scuseria, and Ernzerhof (HSE),[22] which was implemented in the Vienna Ab initio Simulation Package (VASP) code.[23] In the HSE approach, the Coulomb potential in the exchange energy of the Perdew, Burke, and Ernzerhof (PBE)[24] functional is divided into short-range and long-range parts with a screening length of 10 Å. The long-range part and correlation potential are represented by the PBE functional, while the short-range part is mixed with the non-local Hartree–Fock (HF) exchange. We reproduced the experimental band gap of STO (3.25 eV) by using the HF mixing parameter of 28%. The HSE functional has been shown to improve the band gap of semiconductors and give a good description of the electronic structure and formation energies of defects and impurities.[25,26] The cutoff energy of 400 eV was used for the plane-wave basis set. The defect calculations were performed using a $(3 \times 3 \times 2)$ 90-atom supercell and a $2 \times 2 \times 2$ grid of Monkhorst-Pack special *k* points for the Brillouin zone integration. The effects of spin polarization were included in all calculations involving unpaired electrons.

The solubility of a donor-type impurity must be sufficiently high under a given sample growth condition. The formation

energy is the key quantity that must be calculated to investigate the stability of a dopant, and is given by the following equation:

$$E^f(X_{Ti}^q) = E_{tot}(X_{Ti}^q) - E_{tot}(STO) + \mu_{Ti} - \mu_X + q\varepsilon_F \quad (1)$$

Here, $E_{tot}(X_{Ti}^q)$ is the total energy of a STO supercell containing an impurity X (X = Ta, Sb, Nb, or V) at the Ti site with q charge state, and was obtained by our density-functional calculations with a 90-atom supercell in the same way as that in case of Cr doping.[15] $E_{tot}(STO)$ is the total energy of perfect STO, obtained using the same supercell. ε_F is the Fermi level referenced to the bulk VBM, which corresponds to the energy of the electron reservoir for charged impurities. A correction was applied to ε_F to account for the difference in electrostatic potential between the bulk and the defect-supercell.[27] The impurity X was taken from a reservoir with energy μ_X, and the substituted Ti atom was placed in a reservoir with energy μ_{Ti}. The energies μ_X and μ_{Ti} thus represent the chemical potentials, and depend on the experimental growth or annealing conditions. The procedure for estimating μ_X will be addressed at great length later. When STO is grown under equilibrium conditions, the chemical potentials of the constituent atoms, which are referenced to the values of their elemental forms, must satisfy the equilibrium condition $\mu_{Sr} + \mu_{Ti} + 3\mu_O = \Delta H_f(STO) = -16.2$ eV, where $\Delta H_f(STO)$ is the formation enthalpy of STO. The formation of unwanted compounds, such as SrO, can be avoided by imposing the condition $\mu_{Sr} + \mu_O < \mu_{SrO}$. Similar bounds were imposed for SrO_2, TiO, TiO_2, and Ti_2O_3. Analogous forms of eqn (1) can be written for the substitutional La_{Sr}, Y_{Sr}, and F_O. The above-mentioned conditions yield the range of chemical potentials that allow the stable growth of STO, which can be represented by a domain in the two-dimensional space defined by μ_{Sr} and μ_{Ti} (dark-shaded areas in Fig. 1(b) and 1(c)).

Results and discussion

Here we initially examine the effect of an upward shift of ε_F on the stabilization of Cr_{Ti}^-. Fig. 1(b) and 1(c) illustrate the Cr impurities that give the lowest formation energy at each chemical potential condition of (μ_{Sr}, μ_{Ti}):Cr_{Ti}, Cr substituted for Sr (Cr_{Sr}), and Cr at an interstitial site (Cr_i). These are shown in Fig. 1(b) for $\varepsilon_F = 0.3$ eV (p-type STO) and in Fig. 1(c) for $\varepsilon_F = 3.0$ eV (n-type STO). Here, μ_O is uniquely determined at each point (μ_{Sr}, μ_{Ti}) through the above-mentioned equilibrium condition. For p-type STO, Cr_{Ti}^{2+} and Cr_i^{4+} are the dominant species under the stable growth condition, as illustrated by the dark-shaded domain in Fig. 1(b). By contrast, for n-type STO where ε_F is located near the CBM, the dark-shaded domain is associated only with Cr_{Ti}^- (Fig. 1(c)). This suggests that a higher concentration of Cr_{Ti}^-, which is advantageous for photocatalytic activity, can be obtained under n-type conditions. However, such an n-type condition is not achieved without external doping, as addressed in the following. In order to determine realistic values of the chemical potentials, μ_O was estimated by including contributions from enthalpy and entropy.[28] μ_O is expressed as

$$\mu_O(T, P_0) = \{(H_0 + \Delta H(T)) + T(S_0 + \Delta S(T))\}/2 \quad (2)$$

where the tabulated values for standard O_2 enthalpy at $T_0 = 298$ K and $P_0 = 1$ atm ($H_0 = 8.7$ kJ mol^{-1}) and entropy ($S_0 = 205$ J mol^{-1}) are used, $\Delta H(T) = C_P(T - T_0)$ and $\Delta S(T) = C_P \ln(T/T_0)$. Using the ideal gas law for $T \geq 298$ K, $C_P = 3.5k_B$ is used for the heat-capacity per diatomic molecule. The experimental growth conditions of STO described in ref. 12, at a calcination temperature of 1100 °C and a pressure of 1 atm, yields $\mu_O = -1.57$ eV. The equilibrium growth condition is now given as $\mu_{Sr} + \mu_{Ti} = -16.2 + 3 \times 1.57 = -11.50$ eV, which is represented by the dotted lines in Fig. 1(b) and 1(c). The chemical potentials $\mu_{Ti} = -6.05$ eV and $\mu_{Sr} = -5.45$ eV (represented by solid circles in Fig. 1(b) and 1(c)) then give the least favorable condition for Cr_{Ti}, at the boundary of the shaded domain associated with the stable growth condition.

Here, we address how to estimate the chemical potential of the dopants μ_X, which is an important factor in determining the impurity solubility. Fig. 2 illustrates the thermodynamically stable phases for the relevant transition metal (TM) compounds over the range of possible growth conditions between the O-poor limit ($\mu_O = -5.27$ eV) and the extreme O-rich limit ($\mu_O = 0$). μ_x can be derived from the formation enthalpy of its limiting phase which is subject to an upper bound. For instance, for the realistic growth condition $\mu_O = -1.57$ eV (dashed-dotted line in Fig. 2), μ_{Cr} is determined by the formation enthalpy of Cr_2O_3, that is, $2\mu_{Cr} + 3\mu_O \leq \Delta H_f(Cr_2O_3)$, where the upper bound of $\mu_{Cr} = (\mu_{Cr_2O_3} - 3\mu_O)/2$: if μ_{Cr} is pushed higher than the upper bound, Cr_2O_3 will form in addition to the Cr incorporated in the STO lattice. Using a similar procedure, the upper bound for μ_X where X = Ta, Sb, Nb, V, La, and Y can be determined.

Fig. 3 shows the calculated formation energies of the Cr-related defects for these realistic chemical potentials, indicating that Cr_{Ti} is a more stable form of chromium than the other forms (Cr_{Sr} or Cr_i) for a wide Fermi level range, as we discussed in our previous paper.[15] Under a thermodynamic equilibrium condition, the charge neutrality must be satisfied when the concentrations of the positively charged Cr_{Ti}^+ and the negatively charged Cr_{Ti}^- are balanced. This determines the pinning level of

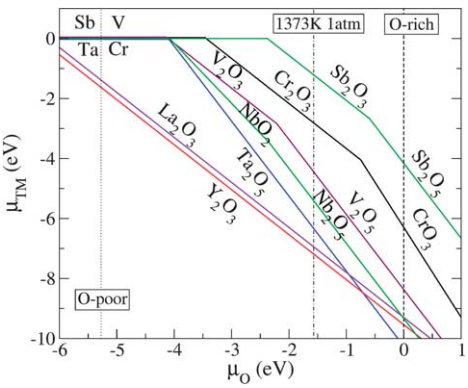

Fig. 2 The relationship between the transition metal (TM) chemical potentials μ_{TM} and the O chemical potential μ_O, as derived from the equilibrium growth of the host: $x\mu_{TM} + y\mu_O = \Delta H_f(TM_xO_y)$. Only the μ_{TM} that gives the upper bound (the lowest μ_{TM}) for the respective μ_O are shown. The dotted-, dashed-, and dashed-dotted vertical lines denote the O-poor ($\mu_O = -5.42$ eV), O-rich ($\mu_O = 0$), and realistic O-rich conditions ($\mu_O = -1.57$ eV), respectively.

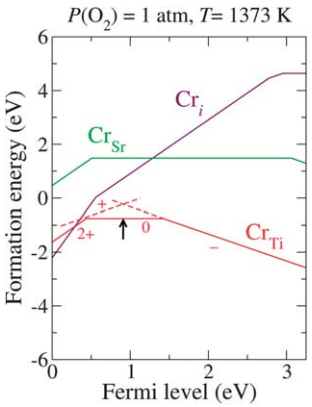

Fig. 3 Calculated formation energy as a function of ε_F for Cr-related defects under a realistic growth condition ($\mu_O = -1.57$ eV). The arrow indicates the estimated pinned ε_F. The slope of each line indicates the charge state. The transition levels between different charge states are denoted as kinks in each plot.

ε_F, shown as an arrow in Fig. 3. Here, the neutral Cr_{Ti}^0, which is likely to act as an electron trapping center,[15] is the predominant charge state at the pinned ε_F. To stabilize the favorable charge state, Cr_{Ti}^-, the pinning level must be elevated. This motivated us to seek donor dopants that can effectively shift ε_F upwards and stabilize Cr_{Ti}^- without the formation of electron-trapping centers.

First, we explore the group-V elements (V, Nb, and Ta) and another pentavalent element Sb (we include Sb in "group-V" in the following discussion). As the ionic radii of all four dopants are closer to that of Ti than that of Sr, preferential substitution at the Ti site is expected. This is supported, for example, by the fact that the calculated formation energy of Ta_{Sr} is ~7 eV higher than that of Ta_{Ti}. We found that Sb_{Ti}, Ta_{Ti}, and Nb_{Ti} do not introduce in-gap states when positively charged (Sb_{Ti}^+, Ta_{Ti}^+, and Nb_{Ti}^+). For the neutral charge state (Sb_{Ti}^0, Ta_{Ti}^0, and Nb_{Ti}^0), an extra electron occupies the bottom of the conduction band, which consists of an extended state resulting from the perturbation of the Ti-*d* states of the host band induced by the impurity. Fig. 4(a) shows the formation energies of the substitutional group-V impurities, along with that of Cr_{Ti}. We found that the positive charge state is energetically stable for Sb_{Ti}, Ta_{Ti}, and Nb_{Ti} over the entire range of ε_F positions in the band gap. The transition levels at which the stable charge state changes from 1+ to 0, $\varepsilon(+/0)$, were found to be located just above the CBM for Sb_{Ti}, Ta_{Ti}, and Nb_{Ti} (not shown in Fig. 4), indicating that they act as shallow donors in STO. By contrast, V_{Ti} creates deep levels in the band gap as characterized by the transition levels $\varepsilon(+/0)$, $\varepsilon(0/-)$, and $\varepsilon(-/2-)$. The in-gap states originate from the vanadium t_{2g} orbitals and are likely to give rise to carrier-trapping centers.

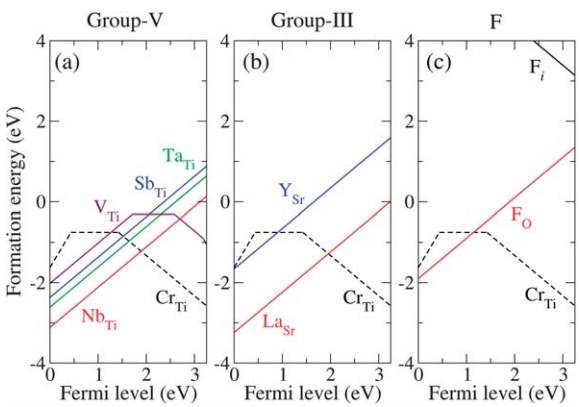

Fig. 4 Calculated formation energies as a function of ε_F for (a) group-V codopants (Nb, Ta, Sb, and V), (b) group-III codopants (La and Y), and (c) F, as well as Cr_{Ti} in each case. All formation energies were calculated for $\mu_O = -1.57$ eV.

For the group-III codopants, we focused on the Sr site for the substitution, because the calculated formation energies showed that La preferably substitutes Sr rather than Ti. The formation energies of La_{Sr} and Y_{Sr} shown in Fig. 4(b) indicate that they act as shallow donors. Without forming any impurity states in the band gap, La_{Sr} and Y_{Sr} are unlikely to act as trapping centers for photoexcited electrons. Fig. 4(c) also shows that F_O is a shallow donor in STO. The ionic radius of F^- (1.33 Å) is slightly smaller than that of O^{2-} (1.40 Å), suggesting that O^{2-} is readily substituted by F^-. In a similar fashion to the other shallow donors, the extra electron of F_O^0 was found to occupy the extended state located at the bottom of the conduction band, whereas F_O^+ does not form any in-gap states. We note that interstitial F (F_i) is energetically unstable, having a much higher formation energy than F_O. The density of states (DOS) for Sb_{Ti}, Ta_{Ti}, Nb_{Ti}, La_{Sr}, Y_{Sr}, and F_O in the positive charge state, showing that they do not introduce in-gap states, are shown in the ESI.†

We now discuss the capability of the codopants to stabilize Cr^{3+} and enhance the photocatalytic activity of STO. The first factor to consider is that the codopants should not cause trapping centers for photoexcited electrons. This is true for the Ta, Nb, Sb, Y, La, and F impurities that are incorporated into STO (based on the assumption that the dominant forms of the Ta, Nb, Sb, Y, La, and F impurities are Ta_{Ti}, Nb_{Ti}, Sb_{Ti}, Y_{Sr}, La_{Sr}, and F_O, respectively). By contrast, the incorporated V impurity creates deep states in the gap and should therefore be excluded from the candidate codopants. The second factor to consider when choosing suitable codopants is their solubility. The donor impurities are activated only when their solubility in the host material is sufficiently high. From Fig. 4, it is clear that La_{Sr} has the lowest formation energy (highest solubility) among the examined donors under the realistic growth condition corresponding to $\mu_O = -1.57$ eV, which determines the upper bound of the chemical potential of each dopant as discussed before; Ta_{Ti}, Nb_{Ti}, V_{Ti}, Sb_{Ti}, Y_{Sr}, and La_{Sr} are limited by the formation of the binary metal oxides Ta_2O_5, Nb_2O_5, V_2O_5, Sb_2O_3, Y_2O_3, and La_2O_3, respectively (see Fig. 2). The solubility of F_O is limited by the formation of SrF_2. In other words, the chemical potential of a dopant must be carefully estimated from the limiting phase, since it significantly affects the solubility of the dopant.

In Cr-doped STO, the pinned Fermi level ($\varepsilon_F = 0.92$ eV) is relatively low, and the majority of the Cr_{Ti} is present in the neutral charge state (Cr_{Ti}^0), as mentioned above. Under this condition, the photocatalytic activity of Cr-doped STO is suppressed.[15] Because the photocatalytic activity is triggered when Cr_{Ti}^- is stabilized, an upward shift of the pinned ε_F should

improve the performance of the material. This is made feasible by incorporating a shallow donor that has a sufficiently low formation energy in the positive charge state (for example, La_{Sr}^{+}), thus suppressing the formation of Cr_{Ti}^{0}. Here, ε_F becomes pinned at a higher level ($\varepsilon_F = 1.95$ eV for La_{Sr}) corresponding to the intersection of the lines for La_{Sr}^{+} (positive slope) and Cr_{Ti}^{-} (negative slope) in Fig. 4(b), as a consequence of the charge balance. The same method was used to determine the pinning levels of ε_F for STO codoped with Cr_{Ti}^{-} and the other dopants considered here. The donor impurity with a lower formation energy gives a higher position of the pinning level. The position of the pinning level with respect to VBM significantly affects the relative concentrations of Cr_{Ti}^{0} and Cr_{Ti}^{-}, as shown in Fig. 5.

Under thermal equilibrium, the concentration of Cr_{Ti}^{q} can be expressed as $N_{sites}\exp(-E^f(Cr_{Ti}^{q})/k_BT)$, where N_{sites} ($\sim 1.67 \times 10^{22}$ cm^{-3}) is the number of available Ti sites in STO that can be substituted by Cr atoms. The negative formation energy of Cr_{Ti}, shown in Fig. 3, gives a concentration that is too high for an impurity, indicating that the actual μ_{Cr} is much lower than the upper bound estimated by our calculations; to obtain a positive value of $E^f(Cr_{Ti})$, the actual μ_{Cr} should be at least 0.9 eV lower than the value of μ_{Cr} taken from Cr_2O_3. Therefore, in order to estimate the relative concentrations of Cr_{Ti}^{0} and Cr_{Ti}^{-} for different values of the pinned ε_F (Fig. 5), we consistently added a constant value to the formation energies of the impurities shown in Fig. 4 such that $E^f(Cr_{Ti})$ became positive over the entire range of ε_F. Without the incorporation of the codopant, Cr_{Ti}^{0} remains the predominant species (solid square in Fig. 5). Codoping successfully shifts the pinning level towards the CBM, and the majority of Cr_{Ti} is replaced by the favorable charge state Cr_{Ti}^{-} at the ε_F for Sb_{Ti} substitution. The concentration of Cr_{Ti}^{-} scales exponentially as a function of the pinned ε_F; we found the best and worst dopants for increasing the concentration of Cr_{Ti}^{-} to be La and Y, respectively.

We also investigated the possibility of the formation of a neutral defect-complex by coupling Cr_{Ti}^{-} with a codopant, which can be computed from the binding energy,

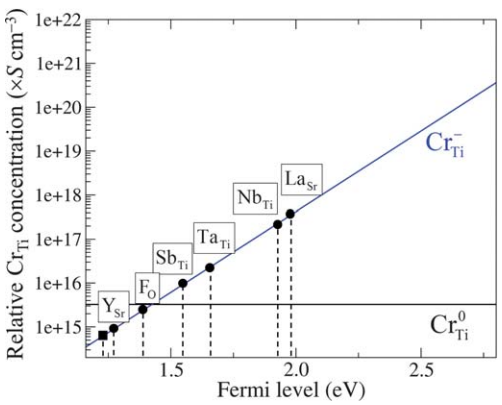

Fig. 5 Calculated relative concentration of Cr_{Ti} defects, derived from hypothetical formation energies, as a function of Fermi level (ε_F). The pinned ε_F results from the charge-neutrality condition for codoped (circles) and non-codoped (square) Cr-doped STO.

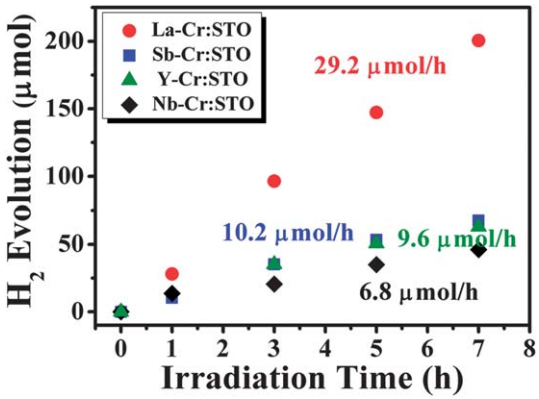

Fig. 6 Photocatalytic H_2 evolution from water splitting of Cr and D codoped $SrTiO_3$ under visible light irradiation, where D = La, Sb, Y, and Nb. All codoped samples were prepared using 5 mol% of Cr and 5 mol% of D.

$$E_b = E^f(Cr_{Ti}^{-}) + E^f(D^{+}) - E^f((Cr_{Ti}\text{–}D)^{0}). \quad (3)$$

Here, $E^f(D^{+})$ is the formation energy of the donor impurity, such as Sb_{Ti}^{+}, and $E^f((Cr_{Ti}\text{–}D)^{0})$ is the formation energy of the Cr_{Ti}–D complex, in which Cr_{Ti}^{-} and D^{+} occupy adjacent sites. A positive value of E_b indicates that the Cr_{Ti}–D complex is lower in energy than the isolated Cr_{Ti}^{-} and D^{+} constituents. We found that the calculated binding energies for all the neutral complexes were relatively small (the highest value was $\sim$0.3 eV). For instance, $E_b((Cr_{Ti}\text{–}La_{Sr})^{0}) = 0.15$ eV, indicating that Cr_{Ti}^{-} and La_{Sr}^{+} experience only a weak driving force to bind to each other. Once Cr and La are incorporated into a sample, under thermal equilibrium (high temperature) they will be confined to their energetically favorable sites (the Ti and Sr sites, respectively); only a small proportion of these dopants will form a complex. This can be clarified as follows. Under equilibrium growth conditions, we can estimate the proportion of the formed Cr_{Ti}–La_{Sr} complex by the following detailed balance:

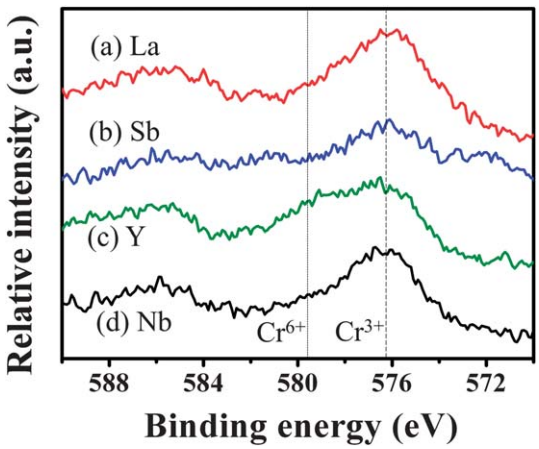

Fig. 7 X-ray photoelectron spectra of Cr 2*p* of (a) La–Cr, (b) Sb–Cr, (c) Y–Cr, and (d) Nb–Cr codoped $SrTiO_3$. The peaks assigned to Cr^{3+} and Cr^{6+} are indicated by dashed and dotted lines, respectively.

$$\frac{[Cr_{Ti}^{-}][La_{Sr}^{+}]}{[(Cr_{Ti}-La_{Sr})^{0}]} = \frac{N_{sites}}{N_{config}}\exp(-E_b/k_BT) \quad (4)$$

where $[Cr_{Ti}^{-}]$, $[La_{Sr}^{+}]$, and $[(Cr_{Ti}–La_{Sr})^{0}]$ are the concentrations of Cr_{Ti}^{-}, La_{Sr}^{+}, and $(Cr_{Ti}–La_{Sr})^{0}$, respectively. N_{config} is the number of configurations of the complex that can be formed, which is 8 for the $Cr_{Ti}–La_{Sr}$ complex. Using the temperature of 1373 K and $[La_{Sr}^{+}] \sim 2.9 \times 10^{17}$ cm^{-3}, determined from the charge-neutrality condition described above, we obtained $[(Cr_{Ti}–La_{Sr})^{0}]/[Cr_{Ti}^{-}] \sim 5.0 \times 10^{-4}$, which means that only 0.05% of Cr_{Ti}^{-} participates in the formation of the complex. During the cooling process, Cr_{Ti}^{-} and La_{Sr}^{+} remain on their sites if they are assumed to be immobile, and thus the proportion of dopants forming a stable complex remains small. Notably, the calculated binding energies of the complexes between the dopants in STO are much smaller than those in TiO_2.[29] Our results show that the incorporated donor impurities in Cr-doped STO are unlikely to form complexes with Cr_{Ti}, and thus can be considered isolated. The photoabsorption properties of the codoped samples can hence still mainly be attributed to Cr_{Ti}^{-}.

Previous experimental results have shown that codoping Cr-doped STO with Ta,[11] Sb,[10] or Nb,[11] significantly enhances the photocatalytic activity, whereas codoping with V[11] decreases the activity, in good agreement with our calculations. It has also been found that Cr^{3+} is stabilized under O-deficient conditions,[30] which enhances the *n*-type condition. Our results are not only applicable to the stabilization of active Cr ions in the Cr-doped STO photocatalyst, but can also provide a route towards the fabrication of *n*-type STO. Our study clearly shows that *n*-type STO can be realized by doping with Nb or La, both of which have high solubility under the realistic growth condition discussed above. Indeed, it has long been realized that doping STO with Nb or La induces a transition from an insulator to an *n*-type semiconductor.[31–33] The dopants Ta, Sb, and Y also act as shallow donors, although their solubility in STO is limited due to their relatively high formation energies compared to those of Nb and La (see Fig. 4). As in other oxides, such as ZnO,[34] F_O is a shallow donor in STO and is highly soluble under O-deficient conditions. By contrast, F_i is a deep acceptor with a high formation energy, and thus cannot contribute to *p*-type conductivity in STO. Theoretical studies of electron-doped STO have also been carried out and are consistent with our results.[19,35]

Now we demonstrate the photocatalytic performance of Cr-doped STO codoped with La, Nb, Sb, and Y, which are theoretically predicted to be the best to the worst codopants for increasing Cr_{Ti}^{-}, in that order. The detail of experiments can be found in the ESI.† We found that all codoped samples can absorb light in the visible region, as shown in Fig. S1.† Fig. 6 shows the photocatalytic activities of Cr-doped STO codoped with La, Nb, Sb, and Y for H_2 evolution from water splitting under visible light irradiation. Cr-doped STO codoped with La (La–Cr:STO) showed the highest activity, in excellent agreement with our theoretical prediction. However, the H_2 evolution activity of Nb–Cr:STO is the lowest, which is inconsistent with our prediction. This discrepancy might result from the presence of other types of Nb-related defects, such as Nb interstitials or its complexes, and the carrier concentration of doped electrons is not sufficiently high to shift the Fermi level up to the expected position under our growth condition. However, the identification of the most stable Nb-related defect in STO is beyond the scope of this work.

In contrast, although the H_2 evolution activity of Sb–Cr:STO was much lower than that of La–Cr:STO, it is still higher than that of Nb–Cr:STO. This could be attributed to the fact that Sb does not have partially filled d states, and thus its related defects, if formed, are unlikely to cause carrier recombination. Y–Cr:STO exhibits H_2 evolution activity comparable to that of the Sb–Cr:STO sample at the beginning of the photochemical reaction. However, the activity gradually decreases with longer irradiation time (Fig. 6). This is qualitatively consistent with our prediction that the activity of Y–Cr:STO is lower than that of Sb–Cr:STO. As mentioned above, the La–Cr:STO possesses the highest amount of Cr_{Ti}^{-} compared to the other codoped samples and thus is a highly active photocatalyst under visible-light irradiation; recently, *via* a synthesis improvement and a reaction-environment modulation, La–Cr:STO was found to exhibit a high quantum yield of 25.6% ($\lambda = 425 \pm 12$ nm) for H_2 evolution,[36] which lends strong support to the findings of our study herein. Next we discuss the effect of donor impurities on the oxidation state of Cr in the codoped samples.

X-ray photoelectron spectroscopy (XPS) measurements were performed to investigate the oxidation state of doped Cr. Fig. 7 shows the XPS spectra of Cr 2*p* of the codoped samples. All the codoped samples showed a peak at about 576.4 eV, which is very close to the peak assigned to Cr^{3+} at 576.7 eV, however, some of our samples showed the peak assigned to Cr^{6+} at 579.2 eV.[10] The relative intensity of XPS allows us to understand the effect of the codopant on the oxidation state of doped Cr as follows. La–Cr:STO and Nb–Cr:STO showed a high peak intensity of Cr^{3+}, while the peaks assigned to Cr^{6+} are almost negligible, in agreement with our calculations that codoping with either La or Nb should efficiently increase the concentration of Cr^{3+}. However, based on our experimental result, codoping with Nb does not enhance the photocatalytic activity even though the concentration of Cr^{3+} is high, indicating that codoping with Nb possibly leads to the formation of other types of defects which cause carrier recombination. Sb–Cr:STO showed a relatively low peak intensity of Cr^{3+}, while a small shoulder of the peak assigned to Cr^{6+} was observed. Y–Cr:STO clearly showed a high peak intensity of Cr^{6+} compared to that of Cr^{3+}, in agreement with our theory (Fig. 5) and experiment (Fig. 6).

Conclusions

In summary, we have systematically studied the capability of several dopants (V, Nb, Ta, La, Y, and F) for the enhancement of the photocatalytic performance of Cr-doped $SrTiO_3$. Based on our density-functional calculations for the stability of the donor-type impurities, La substituted for Sr (La_{Sr}) was predicted to be the best donor for shifting the Fermi level towards the conduction band of $SrTiO_3$. The *n*-type condition is advantageous for increasing the concentration of negatively charged Cr_{Ti}^{-} (Cr^{3+}), which is the key oxidation state for activating

photocatalytic reactions. The prediction from theory has been successfully evidenced by our experiments showing that La and Cr codoped $SrTiO_3$ shows markedly high activity for H_2 evolution from water splitting under visible-light irradiation compared to the other candidate dopants (Nb–Cr, Sb–Cr, or Y–Cr). Furthermore, our computational results show that the other substitutional defects, Sb_{Ti}, Ta_{Ti}, Nb_{Ti}, Y_{Sr}, and F_O, are also shallow donors, although they are less soluble in $SrTiO_3$ than La_{Sr} is, whereas V_{Ti} creates deep states in the band gap and is unable to produce the *n*-type condition. By combining theoretical and experimental investigations, our guiding principle of Fermi level tuning by a codoping scheme was found to be reliable for the design of Cr-doped $SrTiO_3$, and represents a significant step forward in the development of advanced photocatalysts.

Acknowledgements

This work was partially supported by the Japan Science and Technology Agency (JST) Precursory Research for Embryonic Science and Technology (PRESTO) program, and the World Premier International Research Center Initiative on Materials Nanoarchitectonics (MANA), MEXT. P.R. and N.U. thank the High-Performance Computing Center of the California Nano-Systems Institute (CNSI, UCSB) and the Synchrotron Light Research Institute (SLRI, Thailand) for their hospitality. P.R. thanks S. Limpijumnong for the advice.

Notes and references

1 H. Tong, S. Ouyang, Y. Bi, N. Umezawa, M. Oshikiri and J. Ye, *Adv. Mater.*, 2012, **24**, 229–251.
2 A. Fujishima and K. Honda, *Nature*, 1972, **238**, 37–38.
3 A. L. Linsebigler, G. Lu and J. T. Yates, *Chem. Rev.*, 1995, **95**, 735–758.
4 M. S. Wrighton, A. B. Ellis, P. T. Wolczanski, D. L. Morse, H. B. Abrahamson and D. S. Ginley, *J. Am. Chem. Soc.*, 1976, **98**, 2774–2779.
5 A. K. Ghosh and H. P. Maruska, *J. Electrochem. Soc.*, 1977, **124**, 1516–1522.
6 K. Domen, S. Naito, T. Onishi, K. Tamaru and M. Soma, *J. Phys. Chem.*, 1982, **86**, 3657–3661.
7 Y. Xu and M. A. A. Schoonen, *Am. Mineral.*, 2000, **85**, 543–556.
8 R. U. E. 't Lam, L. G. J. de Haart, A. W. Wiersma, G. Blasse, A. H. A. Tinnemans and A. Mackor, *Mater. Res. Bull.*, 1981, **16**, 1593–1600.
9 M. Matsumura, M. Hiramoto and H. Tsubomura, *J. Electrochem. Soc.*, 1983, **130**, 326–330.
10 H. Kato and A. Kudo, *J. Phys. Chem. B*, 2002, **106**, 5029–5034.
11 T. Ishii, H. Kato and A. Kudo, *J. Photochem. Photobiol., A*, 2004, **163**, 181–186.
12 D. Wang, J. Ye, T. Kako and T. Kimura, *J. Phys. Chem. B*, 2006, **110**, 15824–15830.
13 J. W. Liu, G. Chen, Z. H. Li and Z. G. Zhang, *J. Solid State Chem.*, 2006, **179**, 3704–3708.
14 W. Wei, Y. Dai, H. Jin and B. Huang, *J. Phys. D: Appl. Phys.*, 2009, **42**, 055401.
15 P. Reunchan, N. Umezawa, S. Ouyang and J. Ye, *Phys. Chem. Chem. Phys.*, 2012, **14**, 1876–1880.
16 A. Ohtomo and H. Y. Hwang, *Nature*, 2004, **427**, 423–426.
17 D. Kan, T. Terashima, R. Kanda, A. Masuno, K. Tanaka, S. Chu, H. Kan, A. Ishizumi, Y. Kanemitsu, Y. Shimakawa and M. Takano, *Nat. Mater.*, 2005, **4**, 816–819.
18 R. Astala and P. D. Bristowe, *J. Phys.: Condens. Matter*, 2002, **14**, L149.
19 W. Luo, W. Duan, S. G. Louie and M. L. Cohen, *Phys. Rev. B: Condens. Matter Mater. Phys.*, 2004, **70**, 214109.
20 A. Kinaci, C. Sevik and T. Çağin, *Phys. Rev. B: Condens. Matter Mater. Phys.*, 2010, **82**, 155114.
21 R. K. Astala and P. D. Bristowe, *Modell. Simul. Mater. Sci. Eng.*, 2004, **12**, 79.
22 J. Heyd, G. Scuseria and M. Ernzerhof, *J. Chem. Phys.*, 2003, **118**, 8207–8215.
23 G. Kresse and J. Furthmüller, *Comput. Mater. Sci.*, 1996, **6**, 15–50.
24 J. P. Perdew, K. Burke and M. Ernzerhof, *Phys. Rev. Lett.*, 1996, **77**, 3865.
25 A. Janotti, J. B. Varley, P. Rinke, N. Umezawa, G. Kresse and C. G. Van de Walle, *Phys. Rev. B: Condens. Matter Mater. Phys.*, 2010, **81**, 085212.
26 A. Stroppa, G. Kresse and A. Continenza, *Phys. Rev. B: Condens. Matter Mater. Phys.*, 2011, **83**, 085201.
27 C. G. Van de Walle and J. Neugebauer, *J. Appl. Phys.*, 2004, **95**, 3851–3879.
28 J. Osorio-Guillén, S. Lany, S. V. Barabash and A. Zunger, *Phys. Rev. Lett.*, 2006, **96**, 107203.
29 Y. Gai, J. Li, S.-S. Li, J.-B. Xia and S.-H. Wei, *Phys. Rev. Lett.*, 2009, **102**, 036402.
30 S. F. Alvarado, F. La Mattina and J. G. Bednorz, *Appl. Phys. A: Mater. Sci. Process.*, 2007, **89**, 85–89.
31 O. N. Tufte and P. W. Chapman, *Phys. Rev.*, 1967, **155**, 796.
32 T. Tomio, H. Miki, H. Tabata, T. Kawai and S. Kawai, *J. Appl. Phys.*, 1994, **76**, 5886–5890.
33 R. Moos, A. Gnudi and K. Härdtl, *J. Appl. Phys.*, 1995, **78**, 5042.
34 A. Janotti, E. Snow and C. G. Van de Walle, *Appl. Phys. Lett.*, 2009, **95**, 172109.
35 N. Shanthi and D. D. Sarma, *Phys. Rev. B: Condens. Matter Mater. Phys.*, 1998, **57**, 2153.
36 S. Ouyang, H. Tong, N. Umezawa, J. Cao, P. Li, Y. Bi, Y. Zhang and J. Ye, *J. Am. Chem. Soc.*, 2012, **134**, 1974–1977.